A novel heterodimeric cysteine protease is required for interleukin-1β processing in monocytes

Nancy A. Thornberry*, Herbert G. Bull*, Jimmy R. Calaycay†, Kevin T. Chapman‡, Andrew D. Howard†, Matthew J. Kostura§, Douglas K. Miller†, Susan M. Molineaux||, Jeffrey R. Weidner†, John Aunins¶, Keith O. Elliston#, Julia M. Ayala†, Francesca J. Casano||, Jayne Chin§, Gloria J.-F. Ding†, Linda A. Egger†, Erin P. Gaffney*, Guadalupe Limjuco§, Oksana C. Palyha†, S. M. Raju†, Anna M. Rolando||, J. Paul Salley†, Ting-Ting Yamin†, Terry D. Lee, John E. Shively**, Malcolm MacCross‡, Richard A. Mumford†, John A. Schmidt† & Michael J. Tocci||††**

Departments of * Biochemistry, † Biochemical and Molecular Pathology, ‡ Medicinal Chemical Research, § Cellular and Molecular Pharmacology, || Molecular Immunology, ¶ Biochemical Process Research and Development, and # Biological Data, Merck Research Laboratories, PO Box 2000, Rahway, New Jersey 07065, USA

** Beckman Research Institute City of Hope, 1450 East Duarte Road, Duarte, California 91010, USA

Interleukin-1β (IL-1β)-converting enzyme cleaves the IL-1β precursor to mature IL-1β, an important mediator of inflammation. The identification of the enzyme as a unique cysteine protease and the design of potent peptide aldehyde inhibitors are described. Purification and cloning of the complementary DNA indicates that IL-1β-converting enzyme is composed of two nonidentical subunits that are derived from a single proenzyme, possibly by autoproteolysis. Selective inhibition of the enzyme in human blood monocytes blocks production of mature IL-1β, indicating that it is a potential therapeutic target.

INTERLEUKIN-1 (IL-1) is a major mediator in the pathogenesis of chronic and acute inflammatory disease. Evidence that IL-1 is an excellent target for therapeutic intervention has been obtained using macromolecules acting as receptor antagonists (IL-1RA (refs 1–4), soluble IL-1R (ref. 5), anti-IL-1R monoclonal antibodies[6]). But, attempts to identify low-molecular-weight receptor antagonists suitable for oral therapy have been uniformly unsuccessful. Thus another approach, amenable to the design and synthesis of small molecules, is needed.

IL-1β, the predominant form of IL-1 released by human monocytes, is synthesized as an inactive 33K or 31K (M_r 33,000 or 31,000) precursor (pIL-1β)[7,8]. The fully active 17.5K mature form of IL-1β (mIL-1β) begins at Ala 117 and therefore seems to result from processing between Asp 116 and Ala 117 (refs 9, 10). This unique site for prohormone processing is located in an evolutionarily conserved sequence in all known IL-1β molecules[11]. An IL-1β-converting enzyme (ICE) activity has been identified in monocytes and THP.1 cells which cleaves pIL-1β at Asp 116–Ala 117 as well as Asp 27–Gly 28 to yield products of 17.5K and 28K, respectively[12,13]. Cleavage at each site is dependent on aspartic acid in the P_1 position[12,14,15]. Moreover, ICE seems to be a pIL-1β-specific processing enzyme because it does not cleave IL-1α or several other proteins containing many Asp–X bonds[14]. This unique specificity should allow the development of selective inhibitors of ICE.

Here we describe the purification, cloning, specificity, and investigations into the catalytic mechanism of ICE. Potent and selective inhibitors have also been used to affinity-purify active enzyme to homogeneity from THP.1 cell lysates, and to prove the role of ICE in the processing of pIL-1β.

†† To whom correspondence should be addressed.

Purification

ICE was purified from the cytosol of the human monocytic cell line THP.1 by a three-step high-performance liquid chromatography (HPLC) procedure. Sequential fractionation of the cytosolic material over DEAE-5PW and SP-5PW yielded congruent single peaks of ICE activity as measured by cleavage of radiolabelled human pIL-1β[12], a 14-amino-acid peptide spanning the pIL-1β cleavage site[14], or the fluorogenic substrate described below. SDS-polyacrylamide gel electrophoresis (SDS-PAGE) of the SP-5PW peak fractions indicated that two polypeptides with M_r of 22K and 10K consistently chromatographed with ICE activity (Fig. 1*a*). Several preparations purified on SP-5PW also contained small amounts of a protein that migrated with an M_r of 24K (p24) on SDS-PAGE (results not shown). Each fraction containing ICE activity was individually fractionated by reversed-phase HPLC. Two peaks, neither of which retained enzymatic activity (not shown), were observed in direct proportion to the amount of ICE activity injected onto the column. Analysis of the peaks by SDS-PAGE showed that the first peak contained the 22K protein, and the second the 10K protein, in homogeneous form (Fig. 1*b*). Roughly 700 pmol of each protein were purified from 1×10^{11} cells.

Relative molecular masses for the 22K and 10K proteins were determined by on-line liquid chromatography/mass spectral analysis using electrospray ionization[15]. The average M_r values of the purified proteins were 19,866 (Fig. 1*c*) and 10,248 (Fig. 1*d*), respectively, and these were designated p20 and p10.

Substrate specificity

Peptides that span the cleavage site of pIL-1β are suitable substrates for ICE and have been used to define its substrate specificity[14,16]. Two features of peptide substrates are essential for catalytic recognition by the enzyme. First, there is a strong preference for aspartic acid adjacent to the cleavage site, in that any substitution of this residue in pIL-1β and peptide substrates leads to a substantial reduction in the rate of catalysis (>100-fold)[14,16]. The results in Fig. 2 indicate that there is an equally stringent requirement (>100-fold) for four amino-acid residues to the left of the cleavage site, whereas methylamine is sufficient to the right. The results also indicate that broad substitution is tolerated in the P_2 position (peptides 18–24); this has been exploited in the design of peptide substrates and inhibitors described below. The minimal substrate for the enzyme, Ac-Tyr-Val-Ala-Asp-NH-CH_3 (peptide 16; AC, acetyl), is the best peptide substrate yet identified for the enzyme, having a relative

V_{max}/K_m comparable to that for pIL-1β (12±2 versus 10±4 for pIL-1β).

These features are embodied in the fluorogenic substrate, Ac-Tyr-Val-Ala-Asp-7-AMC (peptide 17; AMC, amino-4-methylcoumarin). Cleavage of this substrate shows Michaelis-Menten kinetics with $K_m = 14 \pm 3$ μM. The continuous, fluorometric assay developed with this substrate has facilitated a detailed investigation of the catalytic mechanism of the enzyme.

Classification as a cysteine protease

ICE is inactivated by thiol alkylating reagents[13]. The enzyme is also inhibited by 1,10-phenanthroline (our unpublished observations); however, the mechanism of inhibition is not due to chelation of an active-site metal, but rather to contamination of the phenanthroline with Cu(II) and concomitant metal-catalysed oxidation of an essential thiol[17]. Although such data indicate that the enzyme contains accessible structural and/or catalytic thiol(s), this does not permit assignment of ICE to a protease class.

Three lines of evidence now clearly identify ICE as a cysteine protease. First, and most compelling, is that a diazomethylketone designed with the appropriate active site specificity (Ac-Tyr-Val-Ala-Asp-$COCHN_2$, inhibitor A) is a potent, competitive, irreversible inhibitor of the enzyme. Diazomethylketones are highly selective, covalent inhibitors of cysteine proteases[18]. Addition of ICE to reaction mixtures containing $1 \times K_m$ substrate and 250 nM inhibitor A resulted in time-dependent inhibition of the enzyme (Fig. 3*a*). Irreversible inhibition was demonstrated by the lack of recovery of activity when saturating levels of substrate ($10 \times K_m$) were added to the completely inhibited reaction. The inhibition is strictly competitive, as indicated by the protection against inactivation observed in the presence of saturating substrate ($70 \times K_m$). The second order rate constant for inactivation, $1.64 \pm 0.03 \times 10^4$ M^{-1} s^{-1}, is comparable to those of the best diazomethylketone inhibitors of other cysteine proteases[18,19]. A 10,000-fold smaller value was obtained for the truncated inhibitor Cbz-Asp-$COCHN_2$ (Cbz represents carbobenzyloxy group), consistent with substrate specificity studies.

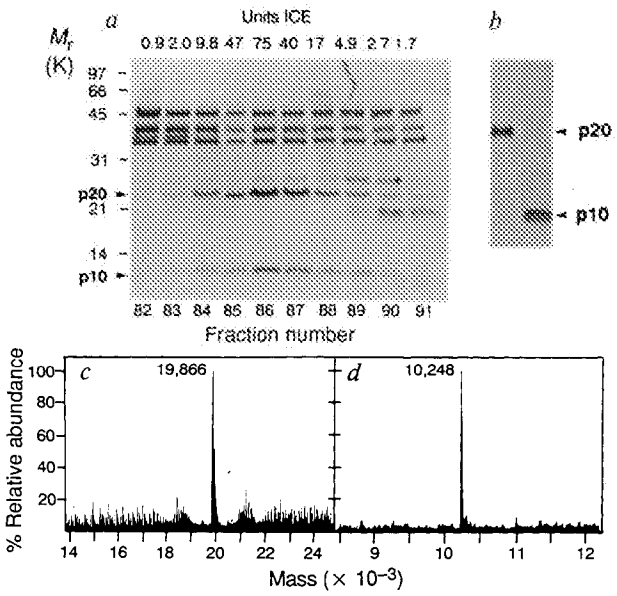

FIG. 1 Identification of ICE proteins. *a*, SDS-PAGE (17–27%) and silver staining of SP-5PW ICE peak fractions (82–91). ICE activity in each fraction as measured in the fluorogenic assay is shown over each lane. Arrows indicate the positions of the 22K and 10K bands that correlated with ICE activity. *b*, SDS-PAGE and silver staining of p20 and p10 ICE proteins purified by reversed-phase HPLC (RP-HPLC). *c*, *d*, The mass of each subunit was determined by mass spectrometry[15]; *c*, 22K subunit (p20); and *d*, 10K subunit (p10).

METHODS. *a*, *b*, ICE activity was measured as described previously[14] and in Fig. 2 legend. THP.1 cells were grown in batch fermenters in Iscove's medium supplemented with 9% horse serum and 0.1–0.3% F68 pluronic, washed in PBS, and broken by dounce homogenization in hypotonic buffer containing 25 mM HEPES, pH 7.5, 5 mM $MgCl_2$, and 1 mM EGTA, 1mM PMSF and 10 μg ml^{-1} pepstatin and leupeptin. After differential centrifugation, the cytosolic extract was clarified by filtration through a 0.22-μm filter, dialysed overnight (5 °C) with 20 mM Tris, pH 7.8, 10% sucrose, 0.1% CHAPS, and 2mM DTT (TSCD buffer). Total protein (3–5 g), corresponding to 1,000 ml cytosolic extract, was applied to a 475-ml bed volume DEAE-5PW HPLC column and eluted with TSCD buffer and a gradient of 0.4 M NaCl and 240 mM Tris-HCl (pH 7.8). Fractions from the DEAE column (50–150 mg) were pooled, diluted with an equal volume of HSCD buffer (contains 25 mM HEPES instead of Tris), adjusted to pH 7.0, applied to a 150-ml bed volume SP-5PW HPLC column and eluted with KCl. Aliquots of SP-5PW fractions were injected onto a narrow bore C4 RP-HPLC column and eluted with a linear gradient of 0.06% trifluoroacetic acid in acetonitrile/H_2O. *c*, *d*, RP-HPLC-purified p20 and p10 (5 pmol) were analysed by capillary liquid chromatography coupled to a Finnigan MAT TSQ-700 triple sector quadrupole mass spectrometer equipped with an electrospray ion source[15].

Amino-terminal truncations

Peptide	P7	P6	P5	P4	P3	P2	P1	P1'	P2'	P3'	P4'	P5'	P6'	P7'	Relative V_{max}/K_m
1	Asn	Glu	Ala	Tyr	Val	His	Asp	Ala	Pro	Val	Arg	Ser	Leu	Asn	1.00 ± 0.05
2		Glu	Ala	Tyr	Val	His	Asp	Ala	Pro	Val	Arg	Ser	Leu	Asn	0.64 ± 0.01
3			Ala	Tyr	Val	His	Asp	Ala	Pro	Val	Arg	Ser	Leu	Asn	0.29 ± 0.02
4				Tyr	Val	His	Asp	Ala	Pro	Val	Arg	Ser	Leu	Asn	0.12 ± 0.00
5			Ac-Tyr	Val	His	Asp	Ala	Pro	Val	Arg	Ser	Leu	Asn		0.81 ± 0.01
6				Ac-Val	His	Asp	Ala	Pro	Val	Arg	Ser	Leu	Asn		<0.005
7					His	Asp	Ala	Pro	Val	Arg	Ser	Leu	Asn		<0.005
8						Asp	Ala	Pro	Val	Arg	Ser	Leu	Asn		<0.005

Carboxy-terminal truncations

Peptide	P7	P6	P5	P4	P3	P2	P1	P1'	P2'	P3'	P4'	P5'	P6'	P7'	Relative V_{max}/K_m
1	Asn	Glu	Ala	Tyr	Val	His	Asp	Ala	Pro	Val	Arg	Ser	Leu	Asn	1.00 ± 0.05
9	Asn	Glu	Ala	Tyr	Val	His	Asp	Ala	Pro	Val	Arg	Ser	Leu		1.22 ± 0.16
10	Asn	Glu	Ala	Tyr	Val	His	Asp	Ala	Pro	Val	Arg	Ser			0.80 ± 0.16
11	Asn	Glu	Ala	Tyr	Val	His	Asp	Ala	Pro	Val	Arg				0.88 ± 0.04
12	Asn	Glu	Ala	Tyr	Val	His	Asp	Ala	Pro	Val					1.02 ± 0.09
13	Asn	Glu	Ala	Tyr	Val	His	Asp	Ala	Pro						1.25 ± 0.15
14	Asn	Glu	Ala	Tyr	Val	His	Asp	Ala							<0.05
15	Asn	Glu	Ala	Tyr	Val	His	Asp	Ala-CO-NH_2							0.93 ± 0.03
16			Ac-Tyr	Val	Ala	Asp-NH-CH_3									12.00 ± 2.00
17			Ac-Tyr	Val	Ala	Asp-AMC									1.9 ± 0.1

P2 substitutions

Peptide	P7	P6	P5	P4	P3	P2	P1	P1'	P2'	P3'	P4'	P5'	P6'	P7'	Relative V_{max}/K_m
18			Ac-Tyr	Val	Ala	Asp	Gly	Trp-NH_2							6.6 ± 0.1
19			Ac-Tyr	Val	His	Asp	Gly	Trp-NH_2							5.4 ± 1
20			Ac-Tyr	Val	Gln	Asp	Gly	Trp-NH_2							4.0 ± 0.3
21			Ac-Tyr	Val	Lys	Asp	Gly	Trp-NH_2							2.5 ± 0.3
22			Ac-Tyr	Val	Phe	Asp	Gly	Trp-NH_2							1.6 ± 0.1
23			Ac-Tyr	Val	Cha	Asp	Gly	Trp-NH_2							0.59 ± 0.08
24			Ac-Tyr	Val	Asp	Asp	Gly	Trp-NH_2							0.34 ± 0.03

FIG. 2 Substrate specificity studies. Peptides that span the cleavage site of pIL-1β were evaluated as substrates and used to define the enzyme's minimum recognition sequence. Values for V_{max}/K_m are expressed relative to peptide 1 and represent the mean ± s.d. ($n = 2$–4). The results indicate that peptide 16 is the minimum recognition sequence for ICE, and that broad substitution is tolerated in P_2.

METHODS. Peptides 1–16 and 18–24 were synthesized using the Merrifield solid-phase technique, purified by RP-HPLC, and confirmed by mass spectral analysis. The fluorogenic substrate, Ac-Tyr-Val-Ala-Asp-AMC (peptide 17), was prepared by conventional solution-phase peptide synthesis. The enzyme used in these studies was purified 100-fold using DEAE ion-exchange chromatography as described in Fig. 1. Peptide cleavage reactions contained 50 units enzyme (1 unit = 1 pmol AMC per min at saturating concentrations of peptide 17) and were done as previously described[14]. In the case of pIL-1β, substrate (33K) and product (17.5K) were separated by SDS-PAGE[12], and quantitated using a radioanalytical imaging system (Ambis Systems).

Second, inactivation of the enzyme by iodoacetate is competitive with substrate (not shown). Competitive inactivation was also demonstrated with other reagents, including cystamine (2-aminoethanethiol disulphide) and glutathione disulphide. Finally, consistent with the enhanced reactivity of catalytic cysteines found in other cysteine proteases[18], the catalytically essential cysteine reacts with [^{14}C]iodoacetate more than 10 times faster than do other cysteines or dithiothreitol (not shown).

The selective and competitive inactivation by [^{14}C]iodoacetate was used to identify the active-site cysteine. On the basis of the rate constant for inactivation of free enzyme by iodoacetate (20 M^{-1} s^{-1}), conditions were chosen for 99% inactivation in the absence of substrate and only 2% in the presence of saturating levels (200 × K_m). The labelling patterns shown in Fig. 3*b* were obtained with enzyme purified 10,000-fold by DEAE-cellulose and sulphylpropyl chromatography. Coomassie blue staining of the gel indicated about 10 major proteins, of which only two, p20 and a band of higher M_r, underwent significant ^{14}C-carboxymethylation. Of these, only p20 was protected by saturating substrate. This established that the catalytically essential cysteine is located in the p20 subunit. Sequencing of a tryptic digest indicated only a single labelled peptide with the sequence Val-Ile-Ile-Ile-Gln-Ala-Cys, with the peak of label coinciding with the cysteine.

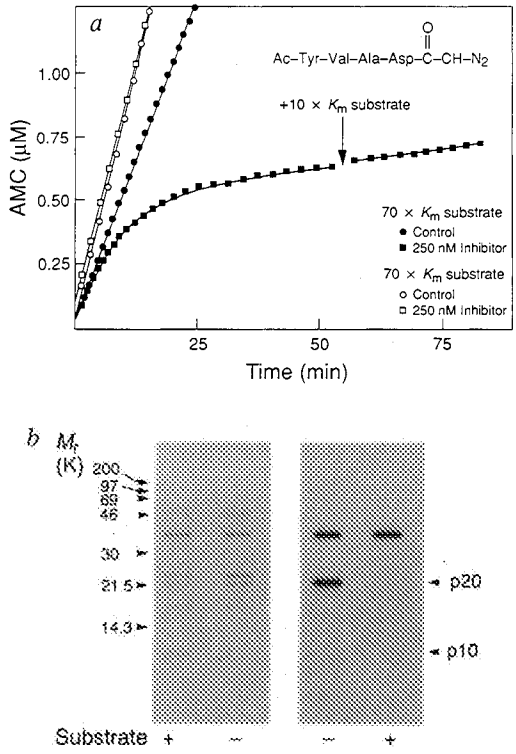

FIG. 3 Evidence that ICE is a cysteine protease. *a*, Inhibition of ICE by the tetrapeptide diazomethylketone, inhibitor A. Addition of peptide A (250 nM) to a reaction mixture containing 1 × K_m substrate resulted in first-order loss of enzyme activity. The solid line is a theoretical fit to the integrated first-order rate equation developed by Morrison[21], yielding a value for the first-order rate constant of 2×10^{-3} s^{-1}, corresponding to a second-order rate constant of 1.6×10^4 M^{-1} s^{-1}. The residual activity observed (<3%) represents background cleavage of the substrate due to contaminating proteases. Addition of saturating levels of substrate (10 × K_m) has no influence on the inhibited velocity, indicating irreversible inhibition. To demonstrate competitive inactivation, an identical experiment was done in the presence of saturating substrate (70 × K_m). *b*, Labelling patterns with [^{14}C]iodoacetate. ICE was labelled with [^{14}C]iodoacetate in the absence (−) and presence (+) of saturating substrate, and analysed by SDS–PAGE. The left-hand lanes are stained with Coomassie blue; the right-hand lanes are autoradiographed. The missing ^{14}C-labelled band in the substrate-protected case identifies the p20 subunit as containing the active-site cysteine.
METHODS. *a*, Ac-Tyr-Val-Ala-Asp-COCHN_2, inhibitor A, was prepared as follows: aspartic acid diazomethylketone β-methyl ester was coupled to Asp-Tyr-Val-Ala using dicyclohexylcarbodiimide (DCC) and hydroxybenzotriazole (HOBt), and the product hydrolysed with triethylamine and water to yield the final product. Reactions (500 μl) contained Ac-Tyr-Val-Ala-Asp-AMC (14 μM or 1 mM) and enzyme (25 units) under standard assay conditions. Reactions were monitored continuously in a spectrofluorometer at an excitation wavelength of 380 nm and an emission wavelength of 460 nm. *b*, Labelling was done on sulphylpropyl-purified enzyme, in solutions containing 1,400 units ml^{-1} enzyme, 100 μM [^{14}C]iodoacetate (56 Ci mol^{-1}), in the standard assay buffer[14] (including dithiothreitol) at 25 °C plus or minus 2.8 mM substrate (200 × K_m), for seven half-lives (40 min).

Reversible inhibition by a peptide aldehyde

The catalytic mechanism of the enzyme suggested that peptide aldehydes would be attractive transition-state analogue inhibitors[20]. This was confirmed with the design and synthesis of Ac-Tyr-Val-Ala-Asp-CHO (inhibitor B), which is a potent, competitive, reversible inhibitor of ICE. It is slow binding, as shown by the slow approach to equilibrium when enzyme was added to reaction mixtures containing inhibitor (50 nM) and 1 × K_m substrate (Fig. 4*a*). Competitive and reversible inhibition was indicated by the recovery of activity observed when saturating levels of substrate (10 × K_m) were added to fully inhibited enzyme. The behaviour of this inhibitor is consistent with a kinetic model in which the rates of association (k_{on}) and dissociation (k_{off}) of enzyme–inhibitor complex are slow compared to rate constants for interaction with the substrate[21]. The k_{on} ($3.8 \pm 0.3 \times 10^5$ M^{-1} s^{-1}) and k_{off} ($2.9 \pm 0.4 \times 10^{-4}$ s^{-1}) define the overall dissociation constant for the equilibrium: $K_i = k_{off}/k_{on} = 0.76 \pm 0.16$ nM. A P_3-substituted aldehyde used as a control in whole-blood studies (see below), Ac-Tyr-D-Ala-Ala-Asp-CHO (inhibitor C), has a 1,000-fold reduced affinity for the enzyme ($K_i = 1.5 \pm 0.1$ μM).

Affinity purification

Affinity chromatography was used to purify active enzyme to homogeneity and to demonstrate the selectivity of the peptide aldehyde inhibitors. The inhibitor Ac-Tyr-Val-Lys-Asp-CHO (inhibitor D), containing lysine at P_2, was synthesized as an affinity ligand and shown to have somewhat lower affinity (K_i = 3 nM) than the original aldehyde, as predicted from substrate studies (Fig. 2, peptide 21).

As anticipated from the enzyme's unusual specificity, the immobilized peptide aldehyde proved to be very selective. Affinity chromatography of a crude THP.1 lysate isolated only two proteins, with M_r values corresponding to p20 and p10 (Fig. 4*b*). Analysis of affinity-purified enzyme by reversed-phase HPLC and amino-terminal sequence analysis indicated that the subunits are present in equimolar ratio (assuming equal extinction coefficients at 214 nm), and confirmed their identity with those described in Fig. 1. Cleavage of internally labelled pIL-1β[12] by affinity-purified ICE yielded mIL-1β with Ala 117 at the N terminus. The affinity chromatography represents a purification of >100,000-fold in a single step. Besides demonstrating the singular specificity of the peptide aldehyde inhibitors, this affinity method provided the first preparations of pure, catalytically active enzyme.

Kinetic evidence that ICE is an oligomer

ICE displays kinetic properties of a dissociable multimeric protein in that the enzyme inactivates on dilution. Dilution of the enzyme by 1,000-fold into a sample containing 1 × K_m substrate results in time-dependent loss of activity ($t_{1/2} = 2.7 \pm 0.4$ h; Fig. 4*c*). Reconcentration (1,000-fold) of the dilute, inactive preparation results in complete recovery of activity (Fig. 4*c*, inset). The most reasonable explanation for this concentration-dependent behaviour is that catalytically active enzyme is composed of at least two subunits and that both subunits are required for

catalytic activity. Dissociation was not observed in the presence of saturating levels of substrate or inhibitor (not shown).

cDNA cloning

N-terminal and internal tryptic peptide sequences from purified p20 or p10 were used to design degenerate oligonucleotide primers for polymerase chain reaction (PCR) amplification of ICE-specific DNA fragments from THP.1 cell cDNA[22]. Separate PCR products for p20 and p10 were subcloned and used as probes to isolate full-length cDNAs from THP.1 and human monocyte libraries. All of the primary phage isolates hybridized with both probes, demonstrating that both ICE proteins were encoded by the same messenger RNA.

Several cDNAs were sequenced to determine the primary structure of ICE (Fig. 5*a*, *b*). There were no significant differences in the cDNA sequences of THP.1 and human monocyte ICE. The longest cDNA insert, which is 1,490 base pairs (bp) long, corresponded to a constitutively expressed, low-abundance transcript (<1:50,000) of 1.6 kilobases (kb) based on northern blot analyses of THP.1 RNA (not shown). The ICE cDNA also hybridized to poly(A) mRNAs of 2.3 and 0.5 kb. All three ICE mRNAs were detected in several non-monocytic cell types including neutrophils and T-lymphocytes, and the Raji B lymphoblastoid cell line (not shown). Five additional nucleotides compared to that of the longest insert were detected by cDNA primer extension (not shown), suggesting that ICE mRNA has a very short 5′ untranslated region (UTR) or secondary structure which limits 5′ extension. The most favourable Kozak consensus sequence (GCCATGG)[23] is at nucleotide 8 and is followed by a long open reading frame (ORF) of 1,212 nucleotides, that terminates with the ochre codon, TAA, at nt 1,220. The cDNA encodes a predicted proenzyme of 404 amino acids (M_r 45,158).

A protein with an M_r of 45K (p45) results from *in vitro* transcription and translation of the full-length ICE cDNA (Fig. 6*b*, lane 1). Two types of ICE cDNAs were identified which differed in the sequence and length of the 3′UTR, suggesting that ICE transcripts are alternatively spliced (not shown).

Primary structure

Amino-acid sequence and mass spectrometry information were used to delineate the regions in p45 corresponding to p20 and p10. Sequence analysis also indicated that p24 was an alternately processed form of p20 (Fig. 5*a*, *b*). From Edman sequencing, the N termini of p24 and p20 are located at Ser 104 and Asn 120, respectively. The N-terminal region of p45 encodes a 119-residue propeptide, containing three cysteines, which lacks the characteristics of a hydrophobic signal sequence. Its function is not known but it is clear from the affinity purification results that it is not required for enzymatic activity (Fig. 4*b*). Asp 297 was predicted as the C-terminus of p20 based on the M_r of the subunit (Fig. 1*c*), identification by fast-atom bombardment mass spectrometry of an appropriately sized Asp-N peptide (Asp 288–Asp 297), and sequence analysis of this peptide by MS/MS[24]. The conclusion that this peptide lies at the terminus of p20 is consistent with the inability of Asp-N to cleave C-terminal aspartic acid residues. The catalytic cysteine identified by active-site labelling, Cys 285, lies within 13 residues of the C terminus of p20.

Sequence analysis of the purified protein and cDNA demonstrated that p10 begins at Ala 317 and terminates with the end of the ORF at His 404. These assignments indicate that a 19-residue spacer separates the C terminus of p20 from the N terminus of p10. Neither this fragment nor the propeptide has been found in purified ICE preparations.

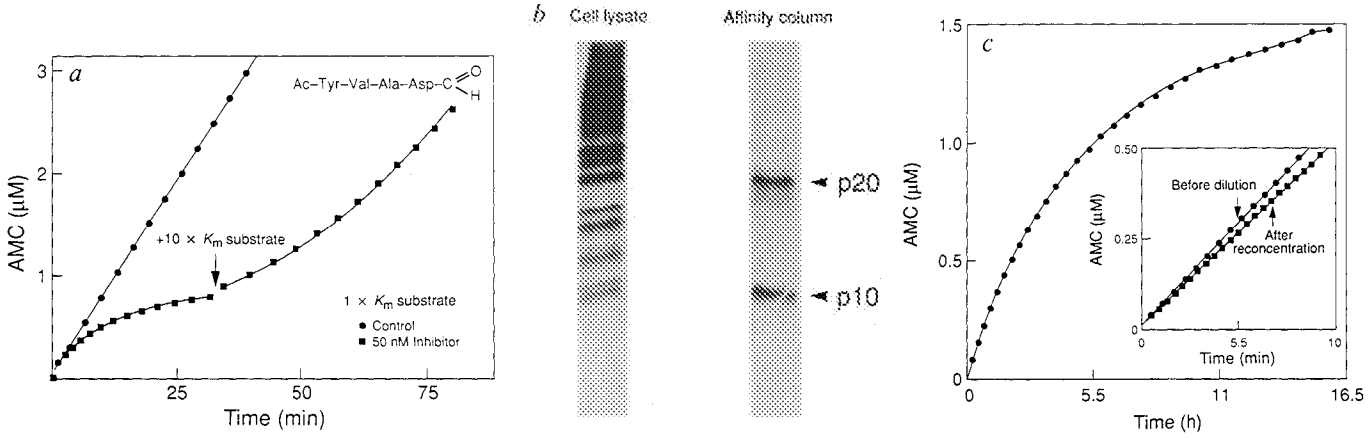

FIG. 4 Potency and selectivity of tetrapeptide aldehydes and evidence that ICE is an oligomer. *a*, Addition of the tetrapeptide aldehyde, peptide B, (50 nM) to a reaction mixture containing $1 \times K_m$ substrate resulted in time-dependent loss of enzyme activity. Addition of saturating levels of substrate ($10 \times K_m$) to the inhibited reaction resulted in slow, first-order recovery of activity, indicating reversible and competitive inhibition. *b*, Affinity chromatography. Silver-stained SDS–PAGE of THP.1 cell lysate applied to the affinity column, and pure ICE eluted by free inhibitor. The procedure gave ~50% recovery of enzymatic activity, and a purification of >100,000-fold. *c*, Reversible inactivation of ICE by dilution. Enzyme (50 μl, 5 units μl^{-1}) diluted 1,000-fold into reaction mixtures containing 14 μM Ac-Tyr-Val-Ala-Asp-AMC ($1 \times K_m$) undergoes reversible dissociation. The solid line is theoretical for a first-order loss of activity with a rate constant of 0.004 min^{-1} (half life, 2.9 h). Less than 2% of the total substrate was consumed over the reaction period. An identical experiment in the absence of sucrose and CHAPS results in a 4-fold faster inactivation rate and both of these components act independently to stabilize the enzyme (not shown). Complete recovery of activity is achieved on 1,000-fold reconcentration of the enzyme. The inset compares the initial velocities before dilution (V_0=0.057 μM AMC min^{-1}) and after concentration (V_0=0.051 μM AMC min^{-1}).

METHODS. *a*, Ac-Tyr-Val-Ala-Asp-CHO, peptide B, was prepared as follows: Alloc-L-aspartic acid β-*t*-butyl ester (Alloc is allyloxycarbonyl) was reduced to the corresponding alcohol through a mixed anhydride using sodium borohydride. The alcohol was oxidized to the aldehyde and converted without purification to the *O*-benzylacylal using trifluoroacetic acid and benzyl alcohol. The Alloc group was removed and the resulting amine coupled *in situ* to Ac-Tyr-Val-Ala using ethyldimethylaminopropylcarbodiimide hydroxybenzotriazole. Hydrogenolysis provided the desired peptide aldehyde. Reactions (500 μl) contained Ac-Tyr-Val-Ala-Asp-AMC (14 μM or 1,000 μM) and enzyme (25 units) under standard assay conditions. The k_{on}, k_{off} and K_i, were calculated according to ref. 21. *b*, The affinity matrix was prepared by coupling the inhibitor D, protected as its dimethyl acetal, to crosslinked Sepharose 4B by established methods[32]. A lysate from THP.1 cells[12] was equilibrated with an equal volume of affinity gel for 5 h at 4 °C, the gel was washed in a column with 100 volumes standard assay buffer, and the enzyme recovered by exchange with 200 μM free inhibitor for 24 h followed by elution with two column volumes of buffer. The enzyme was reactivated by treatment with hydroxylamine and glutathione disulphide, followed by reduction with DTT. *c*, After 20 h, the diluted enzyme (50 ml) was reconcentrated to 50 μl using an Amicon ultrafiltration apparatus (YM10 membrane) and a Centricon-10.

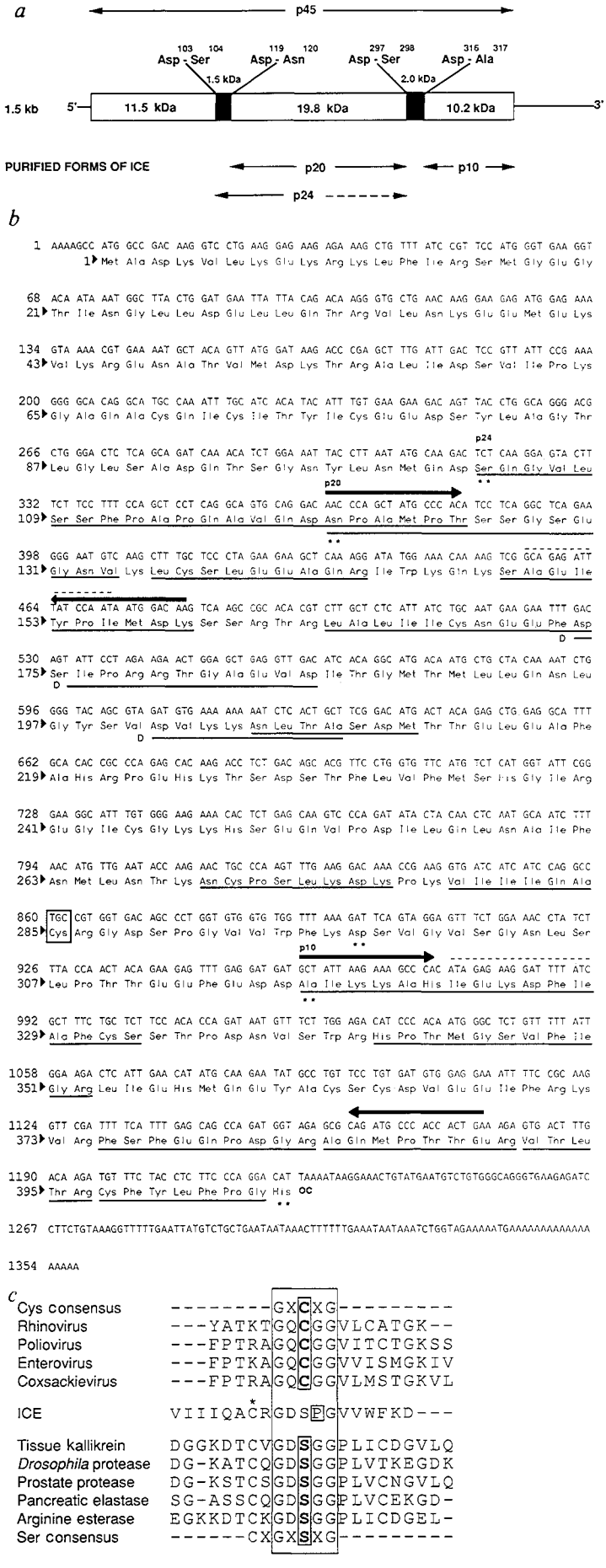

FIG. 5 Organization of the human ICE cDNA. *a*, The predicted ORF encoding the ICE proenzyme (p45) is represented by a rectangle. 5′ and 3′ UTR sequences are shown as solid bars. The four ICE-like cleavage sites flanking the known forms of ICE (p24, p20 and p10) are indicated. The C terminus of p24 has not been determined and is represented by a dashed arrow. *b*, Nucleotide and deduced amino-acid sequence of ICE. Nucleotides are numbered 5′ to 3′. The ochre termination codon is designated OC. Primers used for amplification are denoted by bold arrows. Oligonucleotide probes used to characterize the PCR products are indicated by dashed lines. Deduced sequences confirmed by Edman sequencing are underlined (only a subset are shown for clarity). Asp-N-derived peptides are denoted by D. The N termini of p24, p20 and p10 and the C termini of p20 and p10 are indicated by double asterisks. The active-site Cys is boxed. *c*, Alignments of ICE with cellular serine and viral cysteine proteases. ICE is aligned with the highest scoring sequences from the final Profile searches. Serine and viral cysteine active-site consensus sequences[25,26] and the corresponding sequence in ICE are boxed. Shaded boxes indicate the active-site cysteine or serine residues. The asterisk denotes the catalytic Cys 285 of ICE. Serine protease sequences are tissue kallikrein from mouse (A05308), a serine protease from *Drosophila melanogaster* (PS0049), a prostate-specific protease (S03604), pancreatic elastase (A23473), and arginine esterase (S00613). Viral cysteine protease sequences are coxsackie virus (GNNYA9), bovine enterovirus (GNNYBE), poliovirus type 1 (GNNY1P) and human rhinovirus type 14 (GNNYH4).

METHODS. *a* and *b*, p20 and p10 were reduced, alkylated and sequenced as described previously[33]. For p20, the N-terminal primer, GAYCCNGCNATGCCNAC, was 128 times degenerate and the internal primer, TTRTCCATDATNGGRTA, 48 times degenerate (Stanford code[38]). For p10, the N-terminal primer, GCNATHAARAARGCNCA, was 192 times and the internal primer, GTYTACGGNTGNTGNCT, 128 times degenerate. Single-stranded THP 1 cDNA was synthesized from poly(A)$^+$ mRNA and used as a PCR template as described[22]. For p20, a PCR product of 116 bp was confirmed as ICE-specific by hybridization with the oligonucleotide ATIGGRTAIATYTCIGCR. A 221-bp PCR product was verified for p10, with the probe ATIGARAARGAYTTYATIGC. Probes were 5′ end-labelled and hybridized at 33 °C (15 to 20 °C below T_m) as described previously[34]. The subcloned PCR products were sequenced by the chain termination method[35] and used as hybridization probes in separate screenings of commercial (Clontech) THP.1 (λgt10) or human monocyte (λgt11) cDNA libraries[35]. Positive inserts were subcloned and sequenced on both strands[35]. *c*, Homology searches were conducted with the ICE nucleotide and protein sequences against Genbank[36] and PIR[37] using the GCG package[38]. A non-redundant database[39] was used to generate distinct profiles[40] representing the catalytic regions of cellular serine and viral cysteine proteases. These profiles, designed using alignments suggested in ref. 26, were used to search for similar regions in the primary sequence of ICE. PIR sequence identifiers are bracketed.

The theoretical mass for p20 (Asn 120–Asp 297), assuming all five cysteines including the active-site Cys 285 are reduced, is 19,844. The theoretical mass for p10 (Ala 317–His 404), assuming that all four cysteines are reduced, is 10,244. The mass values determined for p20 (19,866) and p10 (10,248) by on-line liquid chromatography/mass spectral analysis (Fig. 1*c*, *d*) are within 0.11 and 0.04%, respectively, of the theoretical values and are in keeping with the accuracy of this technique for proteins of this size (0.01–0.20%)[15]. These results indicate that neither ICE subunit undergoes significant post-translational modification (for example, farnesylation). But the acidic conditions used for reversed-phase HPLC might remove acid-labile groups (such as phosphate). We hypothesize that in non-stimulated THP.1 cells ICE, like pIL-1β[11], is in the cytosol.

The sequence of ICE is not homologous to any known protein, including cellular cysteine proteases. But Ser 289 of ICE and adjacent residues readily aligns with the consensus sequence (Gly-X-Ser/Cys-X-Gly)[25,26] corresponding to the catalytic regions of serine and viral cysteine proteases (Fig. 5*c*). Using this alignment, the catalytic cysteine of ICE, Cys 285, aligns with a conserved cysteine which is normally disulphide-linked in serine proteases.

Functional expression

To verify further the identity of the ICE cDNA, the 1.5-kb insert was cloned into an expression vector, transfected into COS-7 cells, and assayed for ICE activity. Lysates from ICE-transfected cells, but not those from cells transfected with the expression vector alone, cleaved >80% of the pIL-1β to 17.5 and 28K products (Fig. 6*a*, lanes 1 and 2). The 17.5K cleavage product comigrated with mIL-1β produced by incubation of the substrate with affinity-purified ICE (Fig. 6*a*, lanes 4 and 5) and was completely inhibited by inhibitor B (Fig. 6*a*, lane 3). The substrate specificity of the expressed ICE activity was verified by incubating lysates with a pIL-1β cleavage site mutant (Asp 116→Ala) which cannot be cleaved at Ala 116–Ala 117 by ICE[12]. As with native ICE, the activity from the transfectants cleaves the mutant substrate to a 28K product but not to mIL-1β (Fig. 6*a*, lanes 6 and 7)[12].

Processing of p45

The primary sequence of ICE revealed that the N termini of p24 and p10 as well as the N and C termini of p20 result from cleavage of Asp–X bonds, where X equals Ser 104, Asn 120, Ser 298 or Ala 317 (Fig. 5*a*). Human ICE requires Asp in P_1 and prefers small hydrophobic residues (Gly > Ala > Val) in P_1' (ref. 14). But not all proteins with Asp-X bonds are cleaved by ICE, human and murine pIL-1β remaining the only known substrates[14]. Therefore, it was of interest to determine whether active ICE could cleave the proenzyme. The primary ICE translation product, p45, is stable in rabbit reticulocyte lysates for at least 24 h (Fig. 6*b*, lane 1). On the addition of affinity-purified ICE, p45 was cleaved to yield multiple products (Fig. 6*b*, lane 2), all of which are congruent with the purified forms of ICE (p24, p20, p10; Fig. 5*a*) or intermediates predicted to result from single cleavages of the proenzyme. At an inhibitor concentration of 200 nM, cleavage of p45 by affinity-purified ICE was blocked by inhibitor B ($K_i = 0.7$ nM), but not inhibitor C ($K_i = 1$ μM; Fig. 6*b*, lanes 3 and 4), indicating that processing was not due to a contaminating protease.

Effect of peptide aldehyde on mIL-1β release

The potency and selectivity of the tetrapeptide aldehyde, inhibitor B, make it a useful inhibitor with which to test the processing function of ICE in intact blood monocytes. Pulse-chase experiments (Fig. 7*a*) demonstrated that human blood monocytes rapidly synthesize pIL-1β when stimulated with heat-killed *Staphylococcus aureus*[27]. Intracellular pIL-1β chases directly into plasma as mIL-1β with a half-life of 1.5–2.0 h at 30–95% efficiency, depending on the blood donor.

Titration of inhibitor B into human blood caused a dose-dependent decrease in the plasma level of mIL-1β with a 50% inhibitory concentration (IC_{50}) of ~4 μM (Fig. 7*b*, *d*). Although the IC_{50} is 5,000 × K_i, this is consistent with a cytosolic location for ICE and our finding that the peptide aldehyde penetrates cells poorly (unpublished observation). Inhibition was accompanied by a parallel increase in plasma pIL-1β, such that the total amount of secreted IL-1β (mIL-1β + pIL-1β) remained constant within experimental error (Fig. 7*d*). The inhibitor had no effect on the intracellular amounts of immunoprecipitable pIL-1β (not shown).

Several controls indicate the specificity of the inhibition. First, the control aldehyde, inhibitor C ($K_i = 1.5$ μM), was considerably less potent ($IC_{50} > 100$ μM; Fig. 7*c*, *e*). Second, other protease inhibitors capable of penetrating cell membranes, including pepstatin, E-64 ((N-(L-3-transcarboxyoxiran-2-carbonyl)-L-leucyl)-amido(4-guanido)butane), a neutrophil elastase inhibitor[12], and phosphoramidon were without effect at concentrations up to 100 μM. Finally, concentrations of inhibitor B up to 100 μM had no effect on the plasma levels of IL-6, IL-8 and tumour necrosis factor (TNF-α), the latter two of which are proteolytically processed[28,29]. These results indicate that ICE alone is responsible for activation of pIL-1β.

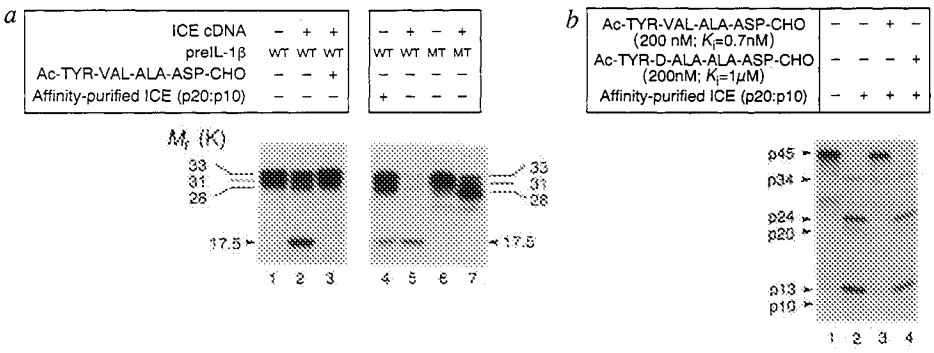

FIG. 6 Functional expression and processing of ICE. *a*, ICE activity in lysates from transiently transfected COS-7 cells. Cells transfected with the ICE cDNA (lanes 2, 3, 5, 7) or control vector (lanes 1, 4, 6) were incubated with wild-type (WT) pIL-1β (lanes 1–5) or the mutant (MT) Ala 116 pIL-1β (lanes 6 and 7) synthesized by *in vitro* translation[12]. ICE-transfected cell lysates were also incubated with the inhibitor B, before substrate addition (lane 3). As a control, affinity-purified ICE (2 units) was added to a lysate from cells transfected with the vector alone (lane 4). The sizes of the pIL-1β (33 or 31K) and the ICE-generated cleavage products (28 and 17.5K) are shown. *b*, p45 is cleaved by affinity-purified ICE. Radiolabelled p45 was synthesized in a rabbit reticulocyte lysate (lane 1) and incubated with 10 units of enzyme (lanes 2–4) either alone (lane 2) or with 200 nM inhibitor B or inhibitor C (lanes 3 and 4). Cleavage was assessed by SDS–PAGE.

METHODS. *a*, The 1.5-kb *Eco*R1 fragment containing the full-length ICE cDNA was cloned into an expression vector under the control of the HIV 5′ LTR. ICE expression plasmid (6 μg) and 0.6 μg of pX8TAT were cotransfected into COS-7 cells (2×10^5 cells, 40 μg Lipofectin) according to the manufacturer's instructions (BRL/GIBCO). Cells were collected 48 h after transfection, lysed in Triton X-100, and assayed for ICE activity[12,14]. *b*, p45-cleavage assays were as follows: 5 μl reticulocyte lysate programmed with T7-transcribed ICE RNA was mixed with 10 units affinity-purified ICE alone or with 200 nM of either inhibitor (18 h, 25 °C) and analysed as described[12].

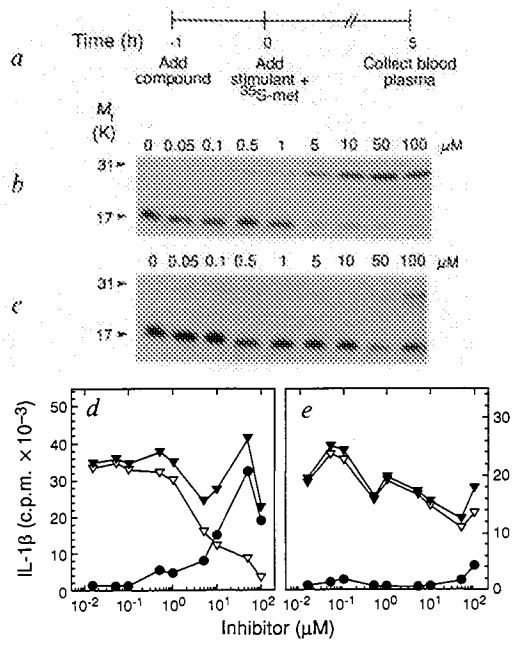

FIG. 7 Inhibition of mature 17.5K IL-1β production by whole human blood monocytes by the tetrapeptide aldehydes, inhibitor B and inhibitor C. *a*, Experimental protocol for pulse-chase experiments. *b*, *c*, SDS–PAGE of immunoprecipitated pIL-1β (31K) and mIL-1β (17.5K) after stimulation of whole blood with heat-killed *S. aureus* (HKSA) in the presence of the indicated concentrations of inhibitor B (*b*) or inhibitor C (*c*). *d*, *e*, Plot of c.p.m. in pIL-1β (●) and mIL-1β (▽) and the total (▼) of both from *b* and *c*, respectively.
METHODS. *a*, Heparinized (10 units ml^{-1}) human blood (1 ml) was incubated with the indicated concentration (μM) of one of two tetrapeptide aldehydes (*b*, *d*, inhibitor B K_i = 0.76 nM; *c*, *e*, inhibitor C, K_i = 1.5 μM), allowed to incubate for 1 h, and then supplemented with 50 μCi [^{35}S]methionine (1,076 Ci mmol^{-1}) and 10^6 colony-forming units per ml. HKSA. *b*, *c*, After incubation at 37 °C, 5 h, the plasma was removed, immunoprecipitated with monospecific rabbit anti-hIL-1β IgG, and analysed by SDS–PAGE and fluorography. *d*, *e*, The 31 and 17.5K bands were counted using a radioanalytical imaging system (Ambis Systems) and plotted versus inhibitor concentration. The c.p.m. in the 17.5K bands were multiplied by 1.86 before plotting to correct for the loss of methionine residues on conversion of pIL-1β to mIL-1β. Total c.p.m. = c.p.m. pIL-1β + corrected c.p.m. mIL-1β.

Discussion

We have defined here the primary structure, molecular organization and catalytic mechanism of ICE, and established its role in the processing of pIL-1β. The enzyme meets all chemical and catalytic criteria for a cysteine protease, but its sequence is not homologous to any known cellular cysteine protease. It is a heterodimer composed of two subunits, p20 and p10. Although p20 contains the catalytic cysteine, kinetic data provide compelling evidence that both subunits are required for catalytic activity.

The subunits, which are proteolytically derived from a single proenzyme, p45, are flanked by Asp-X bonds. This and the observation that p45 is itself an ICE substrate suggest that activation of ICE is, in part, autocatalytic. That p45 was stable after translation *in vitro* rules out an intramolecular autoprocessing mechanism and suggests that p45 is inactive. Activation of ICE presumably requires limited proteolysis by an unidentified protease, in a manner similar to prostromelysin, before autocatalysis can proceed[30]. The detection of ICE activity in transfected COS-7 cell lysates indicates that p45 can also be activated in non-lymphoid cells.

Consistent with the catalytic mechanism and specificity of ICE, the peptide aldehyde transition state analogue, inhibitor B, is a potent, selective inhibitor (K_i = 0.76 nM). The selectivity for ICE was demonstrated by affinity chromatography, which enabled >100,000-fold purification of catalytically active enzyme to homogeneity from THP.1 cells. This inhibitor was used to demonstrate that ICE alone is necessary and sufficient for production of mIL-1β in human blood monocytes stimulated by heat-killed *S. aureus*. A commensurate increase in the plasma level of pIL-1β accompanied inhibition, indicating that secretion of IL-1β is not mechanistically coupled to the processing function of ICE. Furthermore, the released pIL-1β was stable in blood and did not seem to be susceptible to partial activation by proteases, such as cathepsin G, which are capable of cleaving pIL-1β near Asp 116-Ala 117. Nevertheless, it is possible that such 'bystander' proteases exist at sites of inflammation removed from blood[31]. This uncertainty, and the known ability of IL-1α and tumour necrosis factor-α to mediate many of the same biological responses as IL-1β, will require studies *in vivo* to assess fully the therapeutic potential of ICE inhibitors. □

Received 6 December 1991; accepted 16 March 1992.

1. Hannum, C. H. *et al. Nature* **343,** 336-340 (1990).
2. Eisenberg, S. P. *et al. Nature* **343,** 341-346 (1990).
3. Ohlsson, K., Björk, P., Bergenfeldt, M., Hageman, R. & Thompson, R. C. *Nature* **348,** 550-552 (1990).
4. Wakabayashi, G. *FASEB J.* **5,** 338-343 (1991).
5. Fanslow, W. *Science* **248,** 739-742 (1990).
6. McIntyre, K. W. *et al. J. exp. Med.* **173,** 931-939 (1991).
7. Lonnemann, G. *et al. Eur. J. Immun.* **19,** 1531-1536 (1989).
8. Mosley, B. S., Dower, S., Gillis, S. & Cosman, D. *Proc. natn. Acad. Sci. U.S.A.* **84,** 4572-4576 (1987).
9. Cameron, P., Limjuco, G., Rodkey, J., Bennett, C. & Schmidt, J. A. *J. exp. Med.* **162,** 790-801 (1985).
10. Mosley, B. S. *et al. J. biol. Chem.* **262,** 2941-2944 (1987).
11. Schmidt, J. A. & Tocci, M. J. in *Peptide Growth Factors and their Receptors I.* (eds Sporn, M. B. & Roberts, A. B. 473-521 (Springer, Berlin, 1990).
12. Kostura, M. J. *et al. Proc. natn. Acad. Sci. U.S.A.* **86,** 5227-5231 (1989).
13. Black, R. A., Kronheim, S. R. & Sleath, P. R. *FEBS Lett.* **247,** 386-390 (1989).
14. Howard, A. *et al. J. Immun.* **147,** 2964-2969 (1991).
15. Griffin, P. R., Coffman, J. A., Hood, L. E. & Yates, J. R. III *Int. J. Mass Spectrom. Ion Phys.* **111,** 131-149 (1991).
16. Sleath, P. R., Hendrickson, R. C., Kronheim, S. R., March, C. J. & Black, R. A. *J. biol. Chem.* **265,** 14526-14528 (1990).
17. Kobashi, K. & Horecker, B. L. *Archs Biochem. Biophys.* **121,** 178-186 (1967).
18. Rich, D. H. in *Protease Inhibitors* (eds Barrett A. J. & Salvesen, G.) 153-178 (Elsevier, Amsterdam, 1986).
19. Shaw, E. *Adv. Enzym.* **63,** 271-347 (1990).
20. Wolfenden, R. *Nature* **223,** 704-705 (1969).
21. Morrison, J. F. *Trends biochem. Sci.* **7,** 102-105 (1982).
22. Lee, C. C. & Caskey, C. T. *PCR Protocols: A Guide to Methods and Applications* (eds Innis, M. A., Gelfand, D. H., Sninsky, J. J. & White, T. J.) 46-53 (Academic, New York, 1990).
23. Kozak, M. *J. Cell Biol.* **108,** 229-241 (1989).
24. Hunt, D. F., Yates, J. R. III, Shabanowitz, J., Winston, S. & Hauer, C. R. *Proc. natn. Acad. Sci. U.S.A.* **84,** 620-623 (1987).
25. Brenner, S. K. *Nature* **338,** 528-529 (1988).
26. Bazan, J. F. & Fletterick, R. J. *FEBS Lett.* **249,** 5-7 (1989).
27. Schindler, R., Clark, B. D. & Dinarello C. A. *J. biol. Chem.* **265,** 10232-10237 (1990).
28. Perez, C. *et al. Cell* **63,** 251-258 (1990).
29. Clark-Lewis, I., Schumacher, C., Baggiolini, M. & Moser, B. *J. biol. Chem.* **266,** 23128-23134 (1991).
30. Nagase, H., Enghild, J. J., Suzuki, K. & Salvesen, G. *Biochemistry* **29,** 5783-5789 (1990).
31. Hazuda, D. J., Strickler, J., Kueppers, F., Simon, P. L. & Young, P. R. *J. biol. Chem.* **265,** 6318-6323 (1990).
32. Bull, H. G., Thornberry, N. A. & Cordes, E. H. *J. biol. Chem.* **260,** 2963-2972 (1985).
33. Hewick, R. M., Hunkapiller, M. W., Hood, L. E. & Dreyer, W. J. *J. biol. Chem.* **256,** 7990-7997 (1981).
34. Itoh, N., Tanaka, N., Mihashi, S. & Yamashina, I. *J. biol. Chem.* **262,** 3132-3135 (1987).
35. Sambrook, J., Fritsch, E. F. & Maniatis, T. *Molecular Cloning: A Laboratory Manual* (Cold Spring Harbor Laboratory Press, New York, 1989).
36. Bilofsky, H. S. *et al. Nucleic Acids Res.* **14,** 1-4 (1986).
37. George, D. G., Barker, W. C. & Hunt, L. T. *Nucleic Acids Res.* **14,** 11-15 (1986).
38. Devereux, J., Haeberli, P. & Smithies, O. *Nucleic Acids Res.* **12,** 387-395 (1984).
39. Sheridan, R. P. & Venkataraghavan, R. *Proteins* (in the press)
40. Gribskov, M., Homyak, M., Edenfield, J. & Eisenberg, D. *Comput. appl. Biosci.* **4,** 61-65 (1988).

ACKNOWLEDGEMENTS. We thank K. Swiderek for technical assistance, the staff of Merck Visual Communications for preparation of figures, and B. Buckland, P. Davies, J. Demartino, G. Mark III and A. Williamson for their advice and support.

CHEST®

Official publication of the American College of Chest Physicians

Animal Models for COPD*

Steven D. Shapiro

Chest 2000;117;223S-227S
DOI 10.1378/chest.117.5_suppl_1.223S

ISSN:0012-3692

weakness, deconditioning, and impaired gas exchange, play a predominant role to reduced exercise tolerance.[19] A recent study, however, has shown that in COPD there is a strong correlation (r = 0.81) between the resting inspiratory capacity and the exercise capacity.[20] Accordingly, lung function impairment is probably an important cause of decreased exercise tolerance in many COPD patients. Indeed, because of expiratory FL, the maximal VT (and hence ventilation) is closely related to resting inspiratory capacity.[21]

In conclusion, the NEP technique provides a simple and reliable tool for detecting expiratory FL both at rest and during exercise. The method does not require a body plethysmograph, does not depend on patient cooperation and coordination, and can be applied in any desired body posture.

ACKNOWLEDGMENT: We thank Ms. Angie Bentivegna for typing this manuscript.

References

1 Hyatt RE. The interrelationship of pressure, flow and volume during various respiratory maneuvers in normal and emphysematous patients. Am Rev Respir Dis 1961; 83:676–683
2 Gottfried SB. The role of PEEP in the mechanically ventilated COPD patient. In: Roussos C, Marini JJ, eds. Ventilatory failure. Berlin, Germany: Springer-Verlag 1991:392–418
3 O'Donnell DE, Sanii R, Anthonisen NR, et al. Effect of dynamic airway compression on breathing pattern and respiratory sensation in severe chronic obstructive pulmonary disease. Am Rev Respir Dis 1987; 135:912–918
4 Eltayara L, Becklake MR, Volta CA, et al. Relationship of chronic dyspnea and flow limitation in COPD patients. Am J Respir Crit Care Med 1995; 154:1726–1734
5 Leaver DG, Pride NB. Flow-volume curves and expiratory pressures during exercise in patients with chronic airways obstruction. Scand J Respir Dis Suppl 1971; 77:23–27
6 Stubbing DG, Penegelly LD, Morse JLC, et al. Pulmonary mechanics during exercise in subjects with chronic air-flow obstruction. J Appl Physiol 1980; 49:511–515
7 Grimby G, Stiksa J. Flow-volume curves and breathing patterns during exercise in patients with obstructive lung disease. Scan J Clin Lab Invest 1970; 25:303–313
8 Ingram RH Jr, Schilder DP. Effect of gas compression on pulmonary pressure, flow and volume relationship. J Appl Physiol 1966; 47:1043–1050
9 Koulouris NG, Rapakoulias P, Rassidakis A, et al. Dependence of FVC maneuver on time course of preceding inspiration in patients with restrictive lung disease. Eur Respir J 1995; 8:306–313
10 D'Angelo E, Robatto E, Calderini M, et al. Pulmonary and chest wall mechanics in anesthetized paralysed humans. J Appl Physiol 1991; 70:2602–2610
11 Melissinos CG, Webster P, Tien YK, et al. Time dependence of maximum flow as an index of nonuniform emptying. J Appl Physiol 1979; 47:1043–1050
12 Murciano D, Pichot M-H, Boczkowski J, et al. Expiratory flow limitation in COPD patients after single lung transplantation. Am J Respir Crit Care Med 1997; 155:1036–1041
13 Boczkowski J, Murciano D, Pichot M-H, et al. Expiratory flow limitation in stable asthmatic patients during resting breathing. Am J Respir Crit Care Med 1997; 156:752–757
14 Valta P, Corbeil C, Lavoie A, et al. Detection of expiratory flow limitation during mechanical ventilation. Am J Respir Crit Care Med 1994; 150:1311–1317
15 Koulouris NG, Valta P, Lavoie A, et al. A simple method to detect expiratory flow limitation during spontaneous breathing. Eur Respir J 1995; 8:306–313
16 Burrows B, Lebowitz MD. Characteristics of chronic bronchitis in a warm, dry region. Am Rev Respir Dis 1975; 112:365–370
17 Fletcher CM. Bronchitis: an international symposium. Assen, The Netherlands Discussion. Springfield, IL: Charles C. Thomas, 1961; 212–214
18 Jones NG, Jones G, Edwards RHT. Exercise tolerance in chronic airway obstruction. Am Rev Respir Dis 1971; 103: 477–494
19 Gosselink R, Troosters T, Decramer M. Exercise training in COPD patients: the basic questions. Eur Respir J 1997; 10:2884–2891
20 Murariu C, Ghezzo H, Milic-Emili J, et al. Exercise limitation in obstructive lung disease. Chest 1998; 114:965–968
21 Koulouris NG, Dimopoulou I, Valta P, et al. Detection of expiratory flow limitation during exercise in COPD patients. J Appl Physiol 1996; 82:723–731

Animal Models for COPD*

Steven D. Shapiro, MD, FCCP

(CHEST 2000; 117:223S–227S)

Abbreviations: α_1-AT = α_1-antitrypsin; MMP = matrix metalloproteinase; MMP-12−/− mice = macrophage elastase-deficient mice; MMP-12+/+ mice = wild-type mice; NE = neutrophil elastase; PPE = porcine pancreatic elastase

Animal models were critical in ushering in the modern era of COPD, after Gross et al[1] found that intratracheal administration of papain resulted in emphysema in experimental animals. This discovery, combined with the clinical finding by Laurell and Erikkson[2] that patients with α_1-antitrypsin (α_1-AT) deficiency were at increased risk for emphysema, formed the scientific basis for the elastase-antielastase hypothesis for the pathogenesis of emphysema. Today, 35 years later, the elastase-antielastase hypothesis is still the prevailing theory for the development of emphysema, and animal models of COPD remain a critical experimental tool.

Elastase-Induced Emphysema

Since initial experiments of Gross et al,[1] investigators have instilled a variety of proteinases into the lungs of many small and large animals. The administration of porcine pancreatic elastase (PPE; 1 to 4 mg/kg) has produced the most consistent and impressive airspace enlargement in rodents, guinea pigs, dogs, and primates.[3,4] Instillation of PPE results in rapid and significant airspace enlargement, followed by acute neutrophil and subacute

*From the Departments of Pediatrics, Medicine, and Cell Biology and Physiology, Washington University School of Medicine at St. Louis Children's Hospital, St. Louis, MO.
Correspondence to: Steven D. Shapiro, MD, FCCP, Division of Allergy and Pulmonary Medicine, St. Louis Children's Hospital, One Children's Pl, St. Louis, MO 63110; e-mail: shapiro_s@kids.wustl.edu

macrophage accumulation within the lung. Airspace enlargement continues over the first month after instillation and then stabilizes. Elastin content initially decreases, but appreciable elastin messenger RNA expression and elastic fiber deposition, albeit disorganized, is observed within weeks. A more recent study demonstrated by *in situ* hybridization that elastin messenger RNA was strongly expressed in the pleura, blood vessels, and airways following PPE administration. Within the alveoli, expression was observed primarily at the free margins of alveolar septa, with minimal expression in the walls of respiratory spaces.[5] Extracellular matrix repair must be partially effective since lesions are much more severe with the coincident application of β-aminopropionitrile, which prevents elastin and collagen cross-linking.[6] Despite significant airspace enlargement, experimental animals survive. Whether they experience oxygen desaturation with exercise or demonstrate other significant physiologic abnormalities is not known.

The development of emphysema following instillation of other elastases including neutrophil elastase (NE)[7,8] and proteinase-3,[9] but not nonelastolytic enzymes such as bacterial collagenase, further supports the elastase-antielastase hypothesis. Elastase-induced emphysema remains a useful model of emphysema since it is relatively simple to perform and replicates many aspects of the disease. Of course, exposure to cigarette smoke may cause a variety of other abnormalities not observed in this model. Elastase instillation recently has been used to demonstrate that retinoic acid has the capacity to promote alveolarization and lung repair in adult male rats.[10] This model will continue to be most useful in assessing the efficacy of therapeutic agents, particularly those with the capacity to repair lung damage, a critical need in the field.

Other Models

A variety of chemicals and irritants have been used to generate COPD in experimental animals. Interestingly, the administration of lipopolysaccharide results in neutrophil recruitment and airspace enlargement.[4] Yet, humans tolerate bacterial pneumonia without residual emphysema. Whether humans have greater elastic fiber repair capacity or produce enough α_1-AT to limit NE-mediated lung destruction is currently unknown. Cadmium chloride is a chemical agent that has been extensively used to generate airspace enlargement.[4] However, airspace enlargement in this model appears to be secondary to fibrosis with subsequent tethering and enlargement of airspaces. While this has been viewed as a disadvantage of the model, we now appreciate that this mechanism also might be operative in humans with centrilobular emphysema.[11,12] Irritants such as pollutants, oxidants (nitrogen dioxide), and ozone also have been applied to experimental animals. These agents cause airway changes, such as injury to epithelial cells and loss of cilia, but little emphysema. Inorganic dusts, such as silica, have been associated with neutrophil and macrophage accumulation and with emphysema.[13] Severe starvation also has been shown to cause emphysema in animals through unknown mechanism(s).

Natural Genetic Models of Emphysema in Mice

Several mutant mouse strains develop airspace enlargement. These are usually developmental abnormalities rather than ones attributable to the destruction of mature lung tissue that characterizes emphysema. Tight skin (Tsk+/−) mice have a mutation in fibrillin-1, which is involved in elastic fiber assembly.[14] These mice have abnormal airspace development and progressive alveolar enlargement with age. Pallid mice (pa/pa) develop mild emphysema late in life. Beige mice (bg) have a defect in the formation of primary neutrophil granules.[15,16] It remains controversial whether they produce normal levels of serine proteinases and have the capacity to develop emphysema. In addition to these naturally occurring mutations, mice also provide unique opportunities to perform genetic engineering; specifically, manipulation of the mouse genome (see below).

Cigarette Smoke Exposure

Of course, the major environmental factor that predisposes patients to COPD is long-term cigarette smoking. A variety of animals has been exposed to cigarette smoke over the years, including dogs, rabbits, guinea pigs, and rodents.[4,11] Guinea pigs are perhaps the most susceptible species, developing significant airspace enlargement within a few months of cigarette smoke exposure.[17] Rats appear most resistant to emphysema, while, as mentioned, susceptibility in mice appears to be strain dependent.

Murine Model of Cigarette Smoke-Related COPD

We have begun to characterize the similarities and differences between mice and human lungs following chronic cigarette smoke exposure. Using smoking chambers similar to those described in the past for other species,[17] we found that mice tolerate at least two cigarettes per day with carboxyhemoglobin levels of 10 to 14% following smoke exposure.[18] C57BL/6-J mice tolerate cigarette smoke for at least 1 year, although their activity decreases and they occasionally die. Unlike humans, mice are obligate nose-breathers; yet, despite an intricate and extensive nasal sinus pathway, most of their epithelial cells are olfactory in nature without extensive cilia, so that they inefficiently filter tobacco smoke products. Mice have few submucosal glands, which are located exclusively in the trachea. They also contain Clara cells and epithelial cells but lack true goblet cells. In C57BL/6-J and A/J mice at least, ciliated epithelium extend throughout the airway with increased density in proximal airways. In response to 2 months of exposure to cigarette smoke, we observed a loss of ciliated epithelial cells and infiltration of immune and inflammatory cells (T cells, macrophages, neutrophils, and eosinophils), but saw no change in the number of Clara cells (S. Seoane, MD, and S.D. Shapiro, MD; unpublished observations; 1999). We also found that with prolonged cigarette smoke exposure (> 6 months) small airways are occasionally obstructed with inflammatory cells and debris and that there are fewer alveolar attachments. Both of these changes in the small airways have

been hypothesized to contribute to airflow obstruction in COPD.[19,20] Mouse airways have much less extensive branching than those in humans and lack respiratory bronchioles. In alveolar spaces, we observed inflammatory cell recruitment and airspace enlargement in response to cigarette smoke, which is similar to humans. There is increased alveolar duct area and enlarged alveolar spaces[18] (Fig 1). Whether these pathologic changes are associated with abnormal pulmonary function or gas exchange abnormalities awaits further study. We have also observed marked strain-dependent variability with respect to the findings discussed earlier, providing a unique opportunity to uncover COPD susceptibility genes.

Gene Targeting

Soon after the beginning of the next millennium, the sequence of all human genes will be known. However, the function of the proteins encoded by most of these genes will remain a mystery. Transgenic and gene-targeted mice provide powerful techniques that allow investigators to change single variables and, in essence, to perform controlled experiments in mammals, thus determining protein function *in vivo*. Introduction of a linear DNA fragment (transgene) into the pronucleus of one-celled embryos (or more recently into embryonic stem cells) allows the study either of the pattern of expression of that gene or of the biological consequences of overexpression of the protein encoded by the gene in specific tissues. More recently, gene targeting or targeted mutagenesis by homologous recombination in embryonic stem cells has allowed investigators to generate strains of mice that lack individual proteins, providing specific loss of function models.

Mice are used mainly because of their unique capacity to achieve germline transmission of genetic information. Other advantages of the mouse over other experimental animals include a rapid reproductive cycle, large litter sizes, extensive knowledge of mouse biology, abundancy of mouse probes (such as antibodies and complementary DNAs), and lower cost. Importantly, evolutionary conservation has shown us that mice and other mammals are embarrassingly similar to humans. On the other hand, the applicability of these studies to understanding human biology and dissecting the mechanism of disease requires knowledge of similarities and differences with respect to protein profile between mouse and humans. With respect to COPD, long-term cigarette smoke exposure in mice results in many aspects of emphysema, and some aspects of large and small airway diseases that are observed in humans.

Gain-of-Function (Overexpression) Models

The overexpression of collagenase in the lung of transgenic mice that results in airspace enlargement is discussed in the study by D'Armiento et al.[21] Whether collagen degradation alone is responsible for airspace enlargement in these mice remains unclear, but this surprising result raises questions about the intriguing role of collagen turnover in emphysema. Collagen turnover in emphysema is complex. Overall, there is net collagen synthesis in COPD with areas of increased deposition in small airways and depletion in alveolar walls.[12] Further investigation is required to determine whether collagenase inhibition for emphysema will be beneficial or harmful, causing increased small airway fibrosis with increased tethering and enlargement of airspaces.

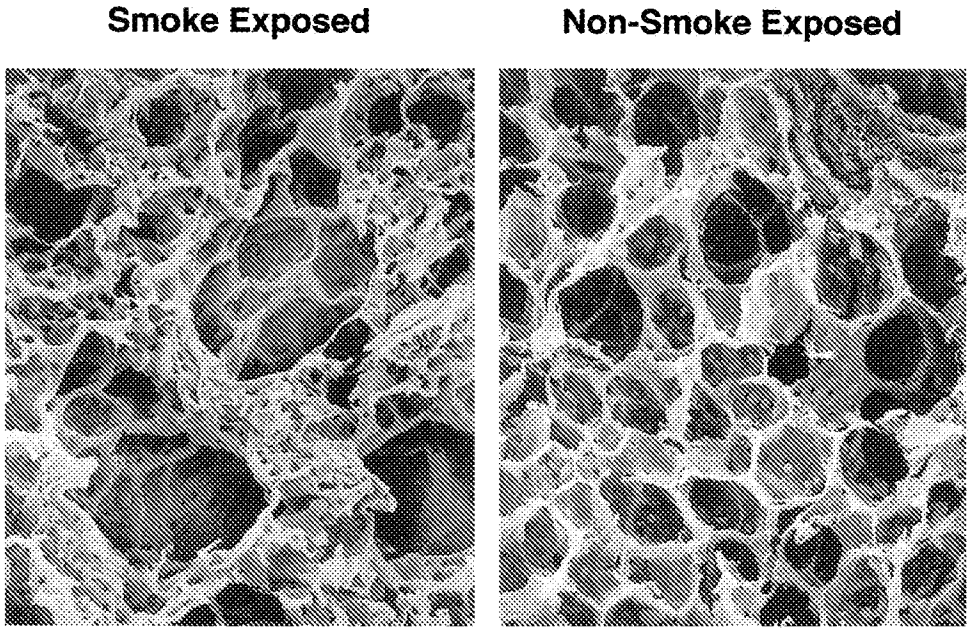

Figure 1. Cigarette smoke-induced airspace enlargement in mice. Scanning electron microscopy (×400) of age-matched C57BL6/J mice either not exposed (*right*) or exposed (*left*) to cigarette smoke for 6 months. Note the airspace enlargement in response to cigarette smoke. Alveolar pores also are increased in size and number (even when corrected for alveolar surface area).

Loss-of-Function (Underexpression) Models

Strains of mice deficient in individual candidate proteinases can be compared to determine their contributions to the development of emphysema in response to cigarette smoke. Macrophage elastase (MMP-12), nearly undetectable in healthy macrophages, is expressed in the alveolar macrophages of human cigarette smokers. MMP-12 also may be detected by immunohistochemistry and *in situ* hybridization in macrophages in patients with emphysema, but not in healthy lung tissue. To determine directly the contribution of macrophage elastase to emphysema, we generated macrophage elastase-deficient (MMP-12−/−) mice by gene targeting,[22] and subjected MMP-12−/− mice and wild-type (MMP-12+/+) littermates to chronic cigarette smoke exposure.[18] In contrast to MMP-12+/+ mice, MMP-12−/− mice did not develop emphysema in response to long-term cigarette smoke exposure. Surprisingly, MMP-12−/− mice also failed to recruit macrophages into their lungs in response to cigarette smoke (Fig 2). Monthly intratracheal instillation of monocyte chemoattractant protein-1 in MMP-12−/− mice exposed to tobacco smoke resulted in recruitment of MMP-12−/− alveolar macrophages but failed to cause airspace enlargement. Thus, MMP-12 is required for both macrophage accumulation and induction of emphysema resulting from chronic inhalation of cigarette smoke. Our current working model is that cigarette smoke induces constitutive macrophages to produce MMP-12 that cleaves elastin, generating fragments that are chemotactic for monocytes. This positive feedback loop perpetuates macrophage accumulation and lung destruction. The concept that proteolytically generated elastin fragments mediate monocyte chemotaxis is not original. Independent studies by Senior et al[23] as well as by Hunninghake et al[24] from the early 1980s demonstrated that elastase-generated elastin fragments were chemotactic for monocytes and fibroblasts. Gene targeting is merely reinforcing this as a major *in vivo* mechanism of macrophage accumulation in a chronic inflammatory condition.

Preliminary evidence using other proteinase-null mice demonstrate that uPA, an MMP activator, and MMP-9 are not involved in the development of cigarette smoke-mediated emphysema in mice. NE-deficient mice developed emphysema only two thirds as often as wild-type mice, suggesting a role for NE in this process (S.D. Shapiro, MD; unpublished manuscript; 1999). We suspect that NE also may be important in small airway changes associated with recurrent infections and neutrophil recruitment.

In summary, the exposure of gene-targeted mice to long-term cigarette smoke demonstrates that macrophage MMPs have the capacity to cause airspace enlargement. Moreover, neutrophils and macrophages have significant

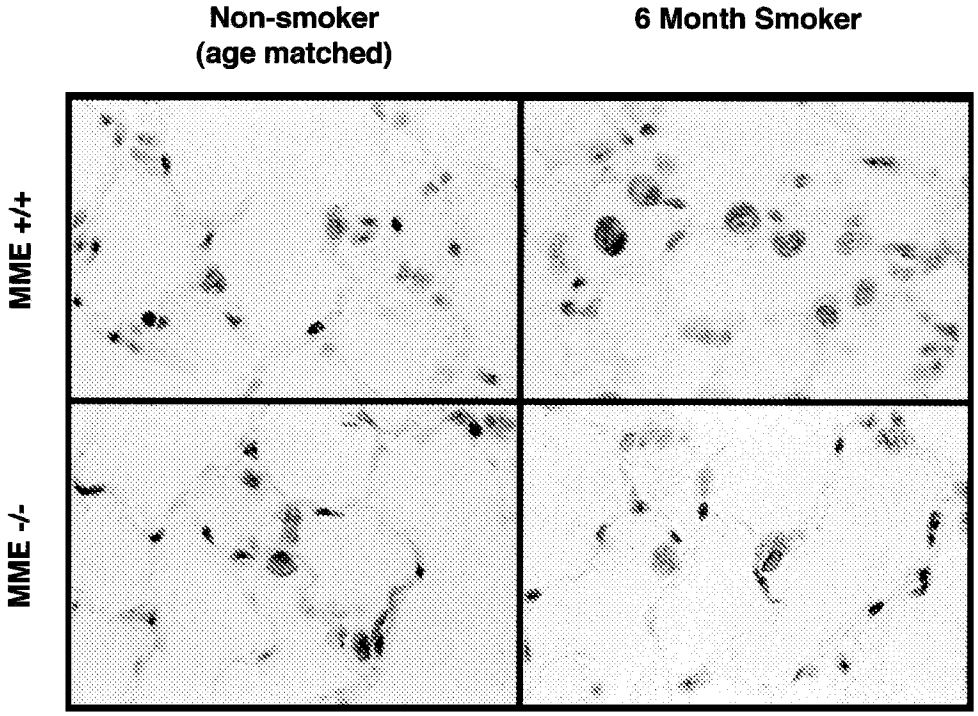

FIGURE 2. MME−/− mice fail to accumulate macrophages in response to cigarette smoke. MME+/+ and macrophage elastase-deficient (MME/null) mice were exposed to cigarette smoke for 6 months. Smoke-exposed mice and age-matched controls then were killed, their lungs were inflated and fixed, and their midsaggital sections were stained for Mac-3. Note that exposure to cigarette smoke resulted in a fourfold increase in the number of alveolar and interstitial macrophages in MME+/+ mice. However, in MME/null mice, while there was an equal number of constitutive macrophages in the lung compared to MME+/+ mice, there was no significant additional recruitment in response to exposure to cigarette smoke.[18]

interactions, with macrophage MMPs degrading α_1-AT and NE degrading tissue inhibitors of metalloproteinases, each augmenting the proteolytic capacity of the other. In addition, NE may activate pro-MMPs into their active form. Finally, macrophages may be required to remove apoptotic neutrophils. Inefficient apoptosis leads to unopposed NE activity and emphysema. One cannot rule out the contribution of T-cells, eosinophils, mast cells, and structural cells of the lung.

Future Utility of Animal Models for COPD

The usefulness of these studies in dissecting the pathogenesis of human disease is directly related to the similarities between human and mouse pathogenesis. Ultimately, as we learn more about mouse and human biology, differences may be as informative as similarities in determining biological pathways. With respect to emphysema, the mouse and human airspaces are quite similar. Mice have less airway branching and lack respiratory bronchioles. Nevertheless, in response to long-term cigarette smoke exposure, several strains of mice develop macrophage-predominant inflammation and airspace enlargement that is similar to those found in humans.[18] Other models, such as elastase instillation, remain quick and useful, especially to begin to identify mechanisms of alveolar repair.

In the future, analysis of murine physiology would be of great assistance in assessing the mouse lesion. In addition, advances in imaging procedures such as CT scans, MRI, positron emission tomography scans, and, ultimately, optical coherence tomography will help to evaluate the pathologic and physiologic changes associated with COPD in mice. The ultimate goal is to utilize the knowledge gained from animal models in treating the many patients who have COPD.

References

1 Gross P, Pfitzer E, Tolker M, et al. Experimental emphysema: its production with papain in normal and silicotic rats. Arch Environ Health 1965; 11:50–58
2 Laurell CB, Erikkson S. The electrophoretic alpha-globulin pattern of serum in alpha-antitrypsin deficiency. Scand J Clin Invest 1963; 15:132–140
3 Kuhn C, Yu S, Chraplyvy M, et al. The induction of emphysema with elastase. Changes in connective tissue. Lab Invest 1976; 34:372–380
4 Snider GL, Lucey EC, Stone PJ. Animal models of emphysema. Am Rev Respir Dis 1986; 133:149–169
5 Lucey E, Goldstein R, Stone P, et al. Remodeling of alveolar walls after elastase treatment of hamsters: results of elastin and collagen messenger RNA *in situ* hybridization. Am J Respir Crit Care Med 1998; 158:555–564.
6 Kuhn C, Starcher B. The effect of lathyrogens on the evolution of elastase-induced emphysema. Am Rev Respir Dis 1980; 122:453–460
7 Janoff A, Sloan B, Weinbaum G, et al. Experimental emphysema induced with purified human neutrophil elastase: tissue localization of the instilled protease. Am Rev Respir Dis 1977; 115:461–478
8 Senior RM, Tegner H, Kuhn C, et al. The induction of pulmonary emphysema induced with human leukocyte elastase. Am Rev Respir Dis 1977; 116:469–477
9 Kao RC, Wehner NG, Skubitz KM, et al. Proteinase 3: a distinct human polymorphonuclear leukocyte proteinase that produces emphysema in hamsters. J Clin Invest 1988; 82: 1693–1699
10 Massaro GD, Massaro D. Retinoic acid treatment abrogates elastase-induced pulmonary emphysema in rats. Nat Med 1997; 6:675–677
11 Snider GL. Emphysema: the first two centuries; and beyond, Part 1. Am Rev Respir Dis 1992; 146:1334–1344
12 Wright JL. Emphysema: concepts under change; a pathologist's perspective. Mod Pathol 1995; 8:873–880
13 Churg A, Hobson J, Wright J. Functional and morphologic comparison of silica- and elastase-induced airflow obstruction. Exp Lung Res 1989; 15:813–822
14 Kielty CM, Raghunath M, Siracusa LD, et al. The tight skin mouse: demonstration of mutant fibrillin-1 production and assembly into abnormal microfibrils. J Cell Biol 1998; 140: 1159–1166
15 Nagle DL, Karim MA, Woolf EA, et al. Identification and mutation analysis of the complete gene for Chediak-Higashi syndrome. Nat Genet 1996; 14:307–311
16 Perou CM, Justice MJ, Pryor RJ, et al. Complementation of the beige mutation in cultured cells by episomally replicating murine yeast artificial chromosomes. Proc Natl Acad Sci USA 1996; 93:5905–5909
17 Wright JL, Churg A. Cigarette smoke causes physiologic and mophologic changes of emphysema in the guinea pig. Am Rev Respir Dis 1990; 142:1422–1428
18 Hautamaki RD, Kobayashi DK, Senior RM, et al. Macrophage elastase is required for cigarette smoke-induced emphysema in mice. Science 1997; 277:2002–2004
19 Hogg JC, Wright JL, Wiggs BR, et al. Lung structure and function in cigarette smokers. Thorax 1994; 49:473–478
20 Lamb D, McLean A, Gillooly M, et al. Relation between distal airspace size, bronchiolar attachments, and lung function. Thorax 1993; 48:1012–1017
21 D'Armiento J, Dalal SS, Okada Y, et al. Collagenase expression in the lungs of transgenic mice causes pulmonary emphysema. Cell 1992; 71:955–961
22 Shipley JM, Wesselschmidt RL, Kobayashi DK, et al. Metalloelastase is required for macrophage-mediated proteolysis and matrix invasion in mice. Proc Natl Acad Sci USA 1996; 93:3942–3946
23 Senior RM, Griffin GL, Mecham RP. Chemotactic activity of elastin-derived peptides. J Clin Invest 1980; 66:859–862
24 Hunninghake GW, Davidson JM, Rennard S, et al. Elastin fragments attract macrophage precursors to diseased sites in pulmonary emphysema. Science 1981; 212:925–927

A Role for Collagenase (Matrix Metalloproteinase-1) in Pulmonary Emphysema*

S. Dalal, PhD; K. Imai, DMD, PhD; B. Mercer; Y. Okada, MD, PhD; K. Chada, PhD; and Jeanine M. D'Armiento, MD, PhD

(CHEST 2000; 117:227S–228S)

Abbreviations: dpc = days postcoitum; MMP = matrix metalloproteinase; RT-PCR = reverse transcriptase-polymerase chain reaction

Animal Models for COPD*

Steven D. Shapiro

Chest 2000;117; 223S-227S
DOI 10.1378/chest.117.5_suppl_1.223S